Results in Physics 73 (2025) 108247

Contents lists available at ScienceDirect

Results in Physics

journal homepage: www.elsevier.com/locate/rinp

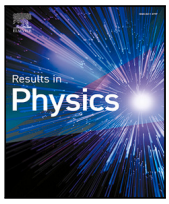

Polydisperse stickiness and particle size on light scattering in dense colloidal suspensions: A numerical study using the binary sticky hard-sphere model

Hiroyuki Fujii [*,1], Koyata Nishikawa, Hyeonwoo Na, Kazumichi Kobayashi, Masao Watanabe

Division of Mechanical and Space Engineering, Faculty of Engineering, Hokkaido University, Kita 13 Nishi 8, Kita-ku, Sapporo, 060-8628, Hokkaido, Japan

ARTICLE INFO

Keywords:
Colloidal suspensions
Particle agglomeration
Light scattering
Dependent scattering theory
Polydispersity in stickiness

ABSTRACT

In nanotechnology using scattered light and colloidal science, it is crucial to model the agglomeration of submicrometer-scale particles and light scattering in dense colloidal suspensions and clarify the quantitative relation between them. We numerically examined the effects of polydisperse stickiness and particle sizes on the scattering properties in the near-infrared optical wavelength using the dependent scattering theory (one of the electromagnetic theory) and bidisperse (binary) sticky hard-sphere (SHS) model at different stickiness parameters and particle sizes. The SHS model has been widely employed as a particle interaction model, but most previous works are for a monodisperse system. Actual suspensions are polydisperse, and our simple bidisperse models allow us to provide a physical interpretation of the two polydisperse effects. We showed that polydisperse stickiness contributions are effectively reduced to monodisperse cases with a mean value of the stickiness parameters. Meanwhile, we showed strong effects of the polydisperse particle size, and its contribution is not reduced to a monodisperse case. At a small particle size (around 100 nm), the polydispersity effects enhance the scattering properties even in the diffusive region of radiative transfer.

Introduction

Dense colloidal suspensions, where colloidal particles are dispersed in a medium, encounter many fields, such as the biomedical, chemical, and food industries [1–5]. In suspensions, particle agglomeration is a key physical phenomenon that influences product qualities (e.g., the qualities of paint and food) [6–9] and relates to colloidal gelation and crystallization [10]. Examples of the particles in agglomerate systems are silica [11,12], titanium dioxide [13], lysozyme (protein) [14], fat globules and proteins in soymilk [15], etc. The particle size ranges from several 10 nm to several micrometers. Particle agglomeration involves a particle configuration change by attractive interaction between particles at a short range [11,12,16,17]. Stronger attractive interaction enhances particle agglomeration, the degree of which is theoretically given by a potential depth or the second Virial coefficient. The dynamic light scattering technique has been widely used to evaluate the agglomeration degree from the effective change of a particle size [18], where its size is in the order of several hundred nanometers and comparable to the optical wavelength. Despite this usefulness, this technique basically requires sample dilution of less than 1% of the volume fraction to hold the Stokes–Einstein relation. Diffuse optical tomography and photon density wave spectroscopy, potentially evaluate agglomeration degree without dilution, although it was developed for evaluating particle size distribution in dilute suspensions [19]. These techniques involve inverse analysis with the radiative transfer and light scattering models to treat strong scattering in dense suspension [20]. In evaluating the agglomeration degree using this technique, modeling a particle configuration change caused by particle agglomeration and light scattering with high physical accuracy is indispensable. Moreover, a physical understanding of their quantitative relationship is crucial in nanophotonics technology.

The dependent scattering theory (DST) has been widely employed as a light scattering model in dense suspension because this electromagnetic theory describes the measurement data of the scattering properties well. The DST uses a particle interaction model to treat the interference between the electric fields scattered by particles. Most studies have employed the hard-sphere (HS) model for a monodisperse system [21–23], but the authors developed it for a polydisperse system [24]. However, the HS model does not treat particle agglomeration because it lacks an attractive part of particle interaction. Recently, Ma et al. investigated the relation between agglomeration and light scattering using the DST with the sticky hard-sphere (SHS) model for a monodisperse system [25]. The monodisperse SHS model treats agglomeration by adjusting the stickiness parameter, which is related to the depth of the attractive potential. Meanwhile, the relation for a

* Corresponding author.
E-mail address: fujii-hr@eng.hokudai.ac.jp (H. Fujii).
[1] He partially conducted this research while he was a visiting scholar at the University of Michigan.

https://doi.org/10.1016/j.rinp.2025.108247
Received 8 January 2025; Received in revised form 31 March 2025; Accepted 1 April 2025
Available online 10 April 2025

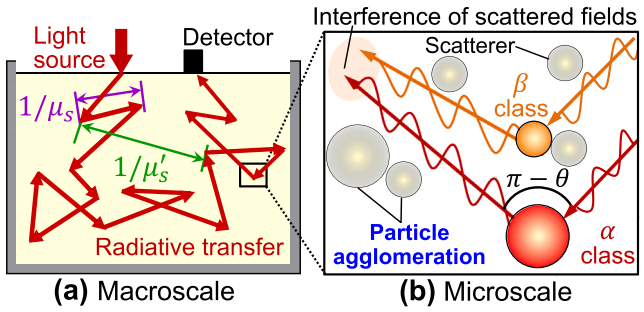

Fig. 1. Schematics of (a) radiative transfer (light propagation) on the macroscopic scale and (b) light scattering on the microscopic scale in a bidisperse stickiness colloidal suspension. μ_s and μ_s' represent the scattering and reduced scattering coefficients.

polydisperse system is still unclear because implementing the polydisperse SHS model is complex. In remote sensing research, Tsang's group has developed the polydisperse SHS model to examine the electromagnetic scattering for snow layers [26,27]. However, there are significant differences in length scales between our system and their system; for example, the wavelength of an electromagnetic wave is in the range of a meter, much longer than the optical wavelength in ours. Their size parameter ($\pi\times$ diameter/wavelength in a medium) is about 1.5 [28], smaller than ours. Thus, it is still necessary to clarify a physical interpretation of the relation between particle agglomeration in polydisperse colloidal suspensions and light scattering at near-infrared wavelength.

We aim to numerically clarify the relation between particle configuration change by agglomeration and light scattering in dense bidisperse (binary) colloidal suspension by the DST with the SHS model. Our simple bidisperse models allow us to provide a physical interpretation of the effects of polydisperse. The polydisperse SHS model can treat two polydispersities: stickiness and particle sizes, where stickiness parameters and diameter depend on particle classes. The total parameter number in a polydisperse system is proportional to the squared total number of particle classes, which makes the appropriate specification more difficult than in a monodisperse system. Hence, investigating the scattering properties at different values of the stickiness parameter is helpful for appropriate modeling. Nevertheless, the two polydisperse effects on light scattering have not been discussed to the best of our knowledge. Motivated by this, we also aim to clarify the two polydisperse effects on light scattering.

Theory and numerical model

This paper mainly considers the scattering and reduced scattering coefficients, μ_s and μ_s', in the light scattering properties (ones of physicochemical properties). The two coefficients correspond to inverse mean free paths of photons in ballistic and diffusive regions on the macroscopic (millimeter) scale, as shown in Fig. 1(a). In the ballistic region near the light source, radiative transfer remains anisotropic, while in the diffusive region far from the source, radiative transfer is effectively isotropic [29–31]. It is noted that the reduced scattering coefficient is of interest to us, while it is less in remote sensing research because of the difference in measurement systems.

We provide general formulations in a polydisperse system with a total number of the particle classes, N_d, although this paper focuses on a bidisperse (binary) system ($N_d = 2$).

Light scattering models

The light scattering model based on the electromagnetic theory considers a colloidal suspension a system consisting of discrete spherical particles suspended in a continuous solvent medium, as shown in Fig. 1(b). The particle size is on the sub-micrometer scale comparable to the near-infrared wavelength. Hence, a single particle scattering is described by the Mie theory [32]. We consider a discrete size distribution and denote a particle class by α or β, *e.g.*, its diameter by d_α or d_β. The indices of α and β run from 1 to N_d. The number-based particle fraction of the α class, f_α, is normalized so that $\sum_{\alpha=1}^{N_d} f_\alpha = 1$.

Dependent scattering theory (DST)

The DST treats the interference between electric fields scattered by particles [21]. The polydisperse DST provides the theoretical formulation of the scattering coefficient as [24]

$$\mu_{s,poly} = \int_0^{2\pi} d\phi \int_0^{\pi} d\theta \sin\theta \sum_{\alpha=1}^{N_d}\sum_{\beta=1}^{N_d} \sqrt{n_\alpha n_\beta}\, \boldsymbol{F}_\alpha^{Mie}(\theta,\phi)\cdot \boldsymbol{F}_\beta^{Mie*}(\theta,\phi) S_{\alpha\beta}(\theta). \tag{1}$$

Here, ϕ and θ are the azimuthal and polar angles, and θ is set to be equal to the scattering angle. n_α (n_β) is the number density for the α class (β class). The number density relates with the volume fraction of particles η as $n_\alpha = \eta f_\alpha / v_p$ with the mean particle volume $v_p = \sum_{\alpha=1}^{N_d} \pi d_\alpha^3 f_\alpha/6$. $\boldsymbol{F}_\alpha^{Mie}$ is the scattering amplitude vector for the α class using the Mie theory, and $\boldsymbol{F}_\beta^{Mie*}$ is the complex conjugate of $\boldsymbol{F}_\beta^{Mie}$. $S_{\alpha\beta}$ is the partial static structure factor (SSF) between the α and β classes. The SSF represents the interference and corresponds to the Fourier transform of the radial distribution function, representing the local particle configuration [33,34]. $S_{\alpha\beta}$ depends on η, n_α, d_α, etc., but we abbreviate the dependence except θ for simple notation. The polydisperse DST results nicely agree with the measurement data [35, 36] for no stickiness cases. The monodisperse DST formulation is given as [21,23]

$$\mu_{s,mono}(d_o) = 2\pi n_0 \sigma_{s,Mie}(d_o) \int_0^{\pi} d\theta \sin\theta \hat{P}_{Mie}(\theta, d_o) S_o(\theta). \tag{2}$$

Here, the number density n_0 is given as η/v_o with the particle volume $v_o = \pi d_o^3/6$ for a monodisperse system. $\sigma_{s,Mie}$ and $\hat{P}_{Mie}$ are the scattering cross section and normalized phase function using the Mie theory. S_o is a monodisperse SSF.

Particle interaction models

Calculating the SSF ($S_{\alpha\beta}$ and S_o) requires the particle interaction model. To investigate the agglomeration and polydispersities in stickiness and particle sizes on light scattering, we considered four models of particle interaction: the hard-sphere (HS) and sticky hard-sphere (SHS) models for bidisperse and monodisperse systems. The polydisperse HS model can treat the polydisperse particle sizes, while the SHS model also treats the polydisperse stickiness.

Hard-sphere (HS) model

We employed the Percus–Yevick model [37] as the HS interaction. The HS interaction considers the strongly repulsive interaction between particles, as shown in Fig. 2(a). When particles contact to each other, they leave by the collision. The details of the formulations and calculations for polydisperse systems are referred to [24,27,38].

Sticky hard-sphere (SHS) model

The SHS model treats the short-range attraction between colloidal particles as a square well type, as shown in Fig. 2(b) and (c). The short-range attraction is induced by entropic depletion force and surfactant additives [10]. The particle attraction causes particle agglomeration (Fig. 2(c)) and changes in particle configuration (particle positions). The SHS model adjusts the degree of the attraction or the potential depth by the so-called stickiness parameter τ. A larger τ-value case corresponds to a less sticky case. The limit of $\tau \to \infty$ corresponds to a

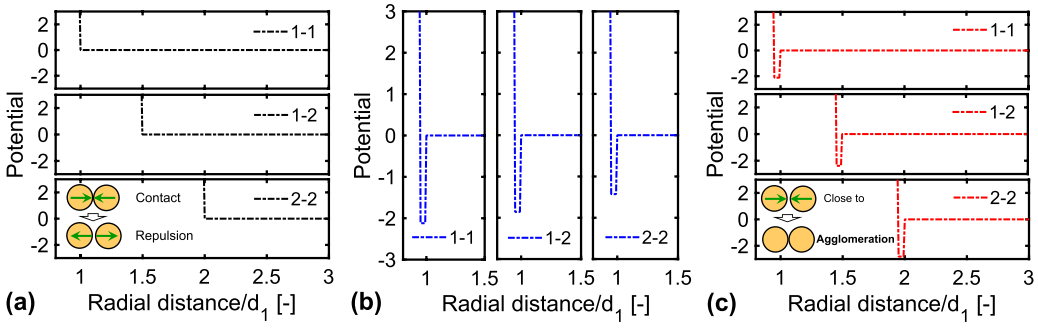

Fig. 2. Particle interaction potentials: (a) HS model for bidisperse particle sizes ($d_2/d_1 = 2.0$), (b) SHS model for bidisperse stickiness ($\tau_{11} = 0.2$, $\tau_{22} = 0.4$) at constant particle size, (c) SHS model for bidisperse particle sizes ($d_2/d_1 = 2.0$) at constant stickiness, $\tau_{\alpha\beta} = 0.2$.

hard-sphere case. The stickiness parameter is significant for thermodynamic quantities, for example, mapping a liquid and gas phase diagram at the stickiness parameters and volume fractions [10].

The polydisperse SHS model has the stickiness parameter, $\tau_{\alpha\beta}$, between the αth and βth particle classes. For polydisperse stickiness, $\tau_{\alpha\beta}$ depends on the particle class pair, and the particle size is constant for the class, as shown in Fig. 2(b). For polydisperse particle sizes, meanwhile, $\tau_{\alpha\beta}$ is constant at all the particle class pairs and the particle size depends on the particle class as shown in Fig. 2(c). Here it is noted in the latter polydispersity, the potential depth depends on the particle class pair despite the constant value of $\tau_{\alpha\beta}$. This is because that the potential depth depends on the particle size in addition to the stickiness parameter; the depth is given by $\log(24\tau_{\alpha\beta}\Delta/(d_\alpha + d_\beta))$ with a potential width Δ (theoretically infinitely small). The parameter is symmetric with the class pair; $\tau_{\alpha\beta} = \tau_{\beta\alpha}$. The total number of the pair combination is $N_d(N_d + 1)/2$. In a bidisperse case, which this paper focuses on, the total number is three (τ_{11}, τ_{12}, and τ_{22}).

The SSF calculation requires a parameter $t_{\alpha\beta}$. A relation between $t_{\alpha\beta}$ and $\tau_{\alpha\beta}$ is given as [27][2]

$$
\begin{aligned}
t_{\alpha\beta}\tau_{\alpha\beta} = {} & \frac{1}{1-\xi_3} + \frac{3d_\alpha d_\beta \xi_2}{(d_\alpha + d_\beta)(1-\xi_3)^2} \\
& - \frac{d_\beta}{(d_\alpha + d_\beta)(1-\xi_3)} \frac{\pi}{24} \sum_{\gamma=1}^{N_d} n_\gamma t_{\alpha\gamma} d_\gamma (d_\alpha + d_\gamma)^2 \\
& - \frac{d_\alpha}{(d_\alpha + d_\beta)(1-\xi_3)} \frac{\pi}{24} \sum_{\gamma=1}^{N_d} n_\gamma t_{\beta\gamma} d_\gamma (d_\gamma + d_\beta)^2 \\
& + \frac{\pi}{576(d_\alpha + d_\beta)} \sum_{\gamma=1}^{N_d} n_\gamma t_{\alpha\gamma} t_{\beta\gamma} (d_\alpha + d_\gamma)^2 (d_\gamma + d_\beta)^2, \qquad (3)
\end{aligned}
$$

where γ denotes the particle class index and $\xi_L = (\pi/6)\sum_{\gamma=1}^{N_d} n_\gamma d_\gamma^L$ ($L = 2, 3$). This relation is also symmetric with the class pair, so that the total number of the equations is $N_d(N_d + 1)/2$. From the above equation, the $t_{\alpha\beta}$ depends on n_α and d_α in addition to the stickiness parameter. In this paper, we solved the quadratic equation (Eq. (3)) to obtain $t_{\alpha\beta}$ by the Broyden method (one of the nonlinear optimization method). Although not shown here, we verified our calculation method in simple cases of quadratic equations where solutions are analytically given.

In the monodisperse SHS model, we solved the single quadratic equation with the stickiness parameter τ_o to attain the t_o-parameter. Then, we calculated the monodisperse SSF, S_o. The details of the calculations are referred to the Refs. [25,27].

Previous research has shown that the SHS model nicely describes experimental data of the SSF using neutron scattering measurements in a system where attractive interaction between particles is considerable, such as silica particles in benzene and silicon oil [11,12,39].

[2] The expression in the text has typos. This paper corrected the expression in the second and fourth terms for the right-hand side about the sum of the diameters.

Table 1
Parameters to specify bidispersity in stickiness and particle size: stickiness parameter $\tau_{\alpha\beta}$, particle fraction f_α, and particle size d_α. $\alpha = 1$, 2 and $\beta = 1$, 2. The subscript of o means a constant value independent of particle classes.

Bidispersity	Parameters		
Stickiness	$\tau_{\alpha\beta}$	$d_\alpha = d_o$	f_α
Particle size	$\tau_{\alpha\beta} = \tau_o$	d_α	f_α

Numerical methods and conditions

We calculated the two scattering coefficients by the DST with the four particle interaction models at different volume fractions. The volume fraction ranges from 1% to 20%, and the optical wavelengths are set as 650, 750, and 850 nm (near-infrared region). Table 1 lists parameters to specify two bidispersities in stickiness and particle size. The particle fraction f_α influences both bidispersities. We calculated τ_{12} as a mean value, $f_1\tau_{11} + f_2\tau_{22}$. We considered two cases of the particle fractions for bidisperse systems: $f_1 = f_2 = 0.5$, $f_1 = 0.7$ and $f_2 = 0.3$. We considered the particle size range from 100 nm to 500 nm, which involves the typical size range of colloidal particles (e.g., fat globules and proteins [15]). Based on the reference data of the fat globules and water, we set the refractive indices of the particle and background medium as 1.44 and 1.33, the same as in our previous study [24]. Our study's size parameter ($\pi\times$ diameter/wavelength in a medium) ranges from 0.5 to 3.2, whose maximum is larger than a typical value of 1.5 in remote sensing of the snow layer [28].

Numerical calculations of the two scattering coefficients (Eq. (1)) using the bidisperse DST for the SHS model require the following input parameters: particle sizes, particle fractions, volume fraction, stickiness parameters, wavelength, and refractive indices of the particle and background medium. We discretized two angles, θ and ϕ. Firstly, we calculated the t-parameters from Eq. (3). Then, we numerically solved a linear matrix equation for the partial SSF at each discrete value of θ [27]. We obtained the integrand of Eq. (1) by combining Mie theory calculations with the SSF results. Finally, we numerically integrated the integrand over the angles using the extended trapezoidal rule to obtain the scattering coefficients. The calculation procedure for the monodisperse DST is almost the same as that for the bidisperse DST calculations. The other details are referred to in our previous study [35].

Although not shown here, we confirmed the verification of our numerical calculations for the monodisperse SHS model; that is, our results of the SSF and light scattering properties agree well with the numerical results by Ma et al. [25]. We also confirmed the verification of our numerical calculations for the polydisperse HS model by comparison with Tsang's group's results [27].

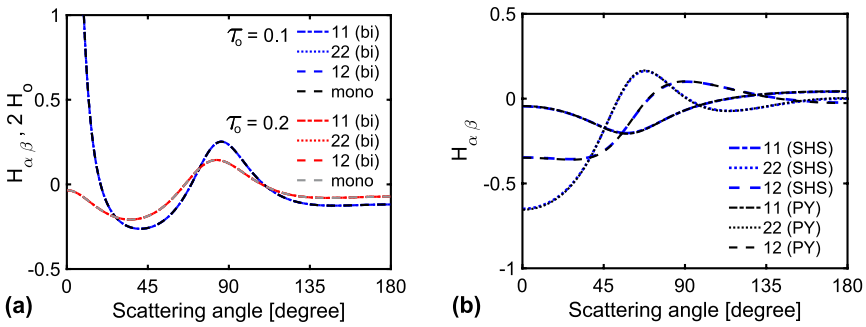

Fig. 3. The TCF, $H_{\alpha\beta}$ and H_o, at the volume fraction of 20% and wavelength of 750 nm: (a) Results of the SHS model for the bidisperse and monodisperse systems at $d_\alpha = d_o = 500$ nm and $\tau_{\alpha\beta} = \tau_o = 0.1$ and 0.2, and (b) Results of the bidisperse SHS model with $\tau_{\alpha\beta} = 15$ and HS models at $d_1 = 250$ nm, $d_2 = 500$ nm, and $f_1 = 0.7$, $f_2 = 0.3$.

Results and discussion

Total correlation function (TCF)

Before the discussion on the scattering properties, we examined the results of the total correlation function (TCF) for the three particle interaction models: monodisperse and bidisperse SHS models and the bidisperse HS model. The TCF is defined as $H_{\alpha\beta} = S_{\alpha\beta} - \delta_{\alpha\beta}$ or $H_o = S_o - 1$ with the SSF. The TCF investigation instead of the SSF is because the TCF at the same class pair is in the same order of magnitude as that at a different class pair, which is convenient for plotting. The TCF results focused on the 20% volume fraction, where the interference between scattered fields is enhanced. Although not shown here, the TCF results are almost zero at less than approximately 5% volume fractions, meaning there is little contribution to the scattering properties. We focused on the results at the wavelength of 750 nm.

Comparison with monodisperse SHS and bidisperse HS models

Firstly, we examined the effects of stickiness on the TCF in two simple cases of the bidisperse SHS model: monodisperse in stickiness and particle sizes and quite a small attractive interaction. Fig. 3(a) compares the bidisperse SHS results at $d_\alpha = d_o$ and $\tau_{\alpha\beta} = \tau_o$ with the monodisperse SHS results. Under the current condition, indices 1 and 2 are just labels, so the bidisperse model has to recover the monodisperse case. The $2H_o$ results are plotted in the figure for the quantitative comparison with the $H_{\alpha\beta}$ results and adjusting the different normalizations in monodisperse and bidisperse systems. All the results agree at each τ_o-value, suggesting the verification of our numerical calculations for the bidisperse SHS model. Fig. 3(b) compares the $H_{\alpha\beta}$ results for the bidisperse SHS model in particle sizes at a large stickiness parameter ($\tau_{\alpha\beta} = 15$) with the bidisperse HS model. The SHS results agree with the HS results at each pair. This result is consistent with the larger stickiness parameter case corresponding to the weaker attractive particle interaction, where agglomeration can be negligible.

As shown in Fig. 3(a), the SHS results have a broad peak at a small scattering angle region ($0 < \theta \lesssim 30$), and the peak value is pronounced at a smaller τ-value. Generally, a positive value of the TCF corresponds to constructive interference between scattered electric fields from particles, while a negative value does to destructive interference. A zero value means no interference. Hence, this result indicates that particle agglomeration induced by attractive interaction enhances constructive interference and forward scattering. Such enhancement has been experimentally observed in systems where particle agglomeration occurs [11,12,16]. Meanwhile, as shown in Fig. 3(b), the HS results do not have such a considerable value at the small angle region.

Polydispersity in stickiness

In Fig. 4, we examined the effects of bidisperse stickiness on the TCF by bidisperse and monodisperse SHS models. In the bidisperse SHS model, we set different $\tau_{\alpha\beta}$ values ($\tau_{11} = 0.2$, $\tau_{22} = 0.4$, $\tau_{12} = f_1\tau_{11} + f_2\tau_{22}$) and the same particle size ($d_1 = d_2 = 500$ nm). In the monodisperse SHS model, we set the particle size to 500 nm and τ_o to $\tau_{\alpha\beta}$, which depends on a particle class pair.

Fig. 4(a) shows the bidsiperse SHS results at the same particle fraction ($f_1 = f_2 = 0.5$). Even at the same particle size and fraction, the $H_{\alpha\beta}$ results differ from each class pair in the small angle region due to the different stickiness degrees. Meanwhile, in the other angle region ($30 \lesssim \theta$), the $H_{\alpha\beta}$ results depend less on polydisperse stickiness, implying that the particle size probably mainly contributes to the TCF. The H_o results are similar to the $H_{\alpha\beta}$ results except for the values in the small angle region, meaning the polydisperse results can be decomposed into a monodisperse contribution for a case of the same particle fraction.

Fig. 4(b) shows the bidsiperse SHS results at different particle fractions ($f_1 = 0.7$, $f_2 = 0.3$). The H_{12} result almost agrees with the H_o result, the same as the case of Fig. 4(a). Meanwhile, H_{11} and H_{22} have peak values different from H_o, although the positions (angles) of crests and troughs are almost identical. This result indicates the difficulty of decomposing that bidisperse results into a monodisperse contribution.

Polydispersity in particle sizes

In Fig. 5, we examined the effects of bidisperse particle sizes on the TCF using the SHS and HS models at the different particle sizes ($d_1 = 250$ nm, $d_2 = 500$ nm) and particle fractions ($f_1 = 0.7$, $f_2 = 0.3$) for constant $\tau_{\alpha\beta}$ values. Both figures show that bidisperse SHS results differ from the HS results at the whole angle region. In the middle angle region ($45 \lesssim \theta \lesssim 90$), negative or positive peak positions for the SHS model are shifted to a larger angle region from those for the HS model. Generally, peak positions appear at a larger angle region at a smaller particle size, so a negative value region before the peak becomes wider [36]. Hence, stickiness for polydisperse particle sizes enhances destructive interference, which is the opposite contribution at the small angle region. Although not shown here, we confirmed that the particle fraction influences the peak positions only slightly while it influences the amplitude of the profile. These results suggest that polydisperse particle size more strongly influences the interference than polydisperse stickiness.

Light scattering properties

We examined the effects of bidisperse stickiness and particle size on the light scattering properties (two scattering coefficients) using the DST with the SHS and HS models. We focused on the results at the wavelength of 750 nm, except for Section "Wavelength dependence".

Polydispersity in stickiness

Fig. 6(a) shows the scattering coefficients (Eqs. (1) and (2)) at different volume fractions to examine bidisperse stickiness on light scattering. Here, we set the particle size, stickiness parameters, and particle fractions the same as in Fig. 4(a). A linear trend of the volume fraction

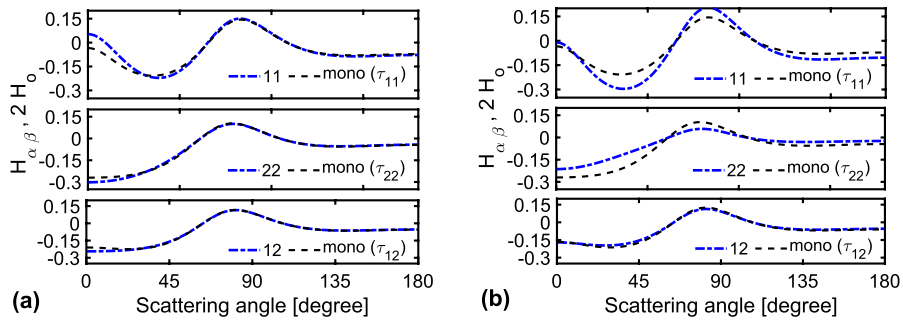

Fig. 4. The TCF for the bidisperse SHS models at the same particle size ($d_1 = d_2 = 500$ nm) and different $\tau_{\alpha\beta}$ values ($\tau_{11} = 0.2$, $\tau_{22} = 0.4$, $\tau_{12} = f_1\tau_{11} + f_2\tau_{22}$), and monodisperse SHS models at $d_o = 500$ nm and $\tau_o = \tau_{\alpha\beta}$ at each class pair: (a) $f_1 = f_2 = 0.5$ and (b) $f_1 = 0.7$, $f_2 = 0.3$. The other details are the same as Fig. 3(a). The corresponding potential is shown in Fig. 2(b).

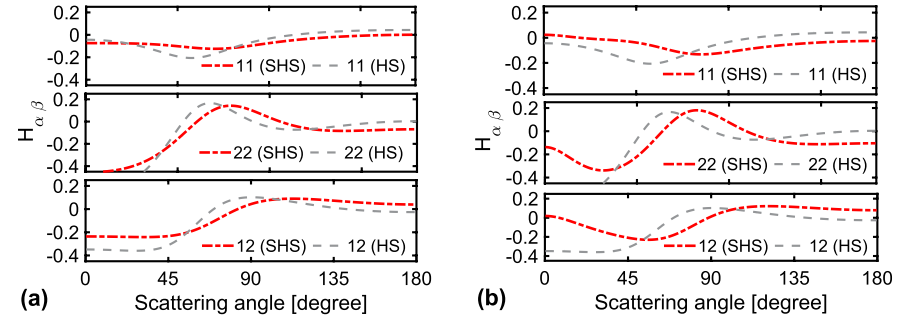

Fig. 5. The TCF for the bidisperse SHS and HS models at the different particle sizes ($d_1 = 250$ nm, $d_2 = 500$ nm) and particle fractions ($f_1 = 0.7$, $f_2 = 0.3$) for the constant $\tau_{\alpha\beta}$ value of (a) 0.4 and (b) 0.2. The corresponding potentials are shown in Fig. 2(a) and (c).

dependence is seen at approximately less than 5%, meaning there is no interference between the scattered electric fields, so-called independent scattering [40]. The results in the small volume fraction region are almost identical among the particle interaction models because the particle interaction influences the SSF and scattering properties little. The curvilinear trend is seen at the region with a more than 5% volume fraction, and it comes from destructive interference via the SSF, known as dependent scattering [20,23].

As shown in Fig. 6(a), the SHS models' results are larger than the HS results at the large volume fraction region. This result is because the constructive interference by particle agglomeration enhances light scattering. As shown in the figure's bottom, a relative difference (RD) in the results between the bidisperse SHS and monodisperse HS models approach to approximately 18% with increasing the volume fraction. For monodisperse SHS models, the coefficient at a smaller τ_o value is larger in the dense region. This result comes from the large value of the TCF or SSF at the small scattering angle, as shown in Fig. 3(a), which contributes to constructive interference. The bidisperse SHS results coincide with the monodisperse SHS results at the mean value of $\tau_{\alpha\beta}$ ($\tau_o = 0.3$). The RDs between the two SHS models are within 1%. This result suggests that polydisperse stickiness less influences the scattering properties due to the fact the scattering coefficient is averaged over the particle class pairs. Although not shown here, the above result is also seen at different particle fractions ($f_1 = 0.7$, $f_2 = 0.3$, the same condition as Fig. 4(b)): there is a nice agreement between the bidisperse SHS and monodisperse SHS models at the mean value ($\tau_o = 0.26$).

Fig. 6(b) shows that the reduced scattering coefficients between models are similar, unlike the scattering coefficient. The RDs between bidisperse SHS and monodisperse HS models are less than 5%. This fact would be explained by a near unity value of the anisotropic factor, g (inset of the figure). The reduced scattering coefficient is given by $\mu_s(1-g)$. Particle stickiness enhances the forward scattering and makes a g-value approach to unity, resulting in a smaller value of $(1-g)$. Hence, the two contributions of μ_s and $(1-g)$ are canceled out. The SHS results are smaller than the HS results, which is opposite the scattering coefficient case. This fact is also due to the anisotropic factor value.

The slight difference in the reduced scattering coefficient between particle interaction models suggests that the stickiness might less influence the diffusive region of radiative transfer. Meanwhile, the authors showed that at a small particle size, the reduced scattering coefficient strongly depends on polydispersity in particle sizes [36]. This fact suggests that the stickiness effect also might depend on the particle size. Fig. 7 show that the two coefficients at a small particle size ($d_1 = d_2 = 130$ nm), where the other conditions are the same as in Fig. 6. The bidisperse SHS results largely differ from the monodisperse HS results, even in the reduced scattering coefficient. The RDs between the two models approach to around 50% in both coefficients. Like the large particle size case, the monodisperse SHS results with the mean stickiness parameter agree well with the bidisperse SHS results. These facts suggest the stickiness itself strongly influences light scattering in the ballistic and diffusive regions.

Polydispersity in particle sizes

In Fig. 8, we examined the effects of bidisperse particle sizes on light scattering. Here, we set the particle size, particle fractions, and stickiness parameters the same as in Fig. 5(b). As shown in Fig. 8(a), unlike polydisperse stickiness (Fig. 6(a)), the scattering coefficients using the monodisperse SHS model with the mean diameter largely differ from the bidisperse SHS results. The difference is seen even in the small volume fraction region, meaning the monodisperse model does not describe independent scattering. The RDs between the bidisperse HS and SHS models are smaller than those between the monodisperse and bidisperse SHS models. These results suggest that polydisperse particle size strongly influences the scattering coefficient over polydisperse stickiness.

As shown in Fig. 8(b), the reduced scattering coefficients for the three models are similar to the bidisperse stickiness case (Fig. 6(b)). The RDs to the bidisperse SHS model are within 6% at the whole volume

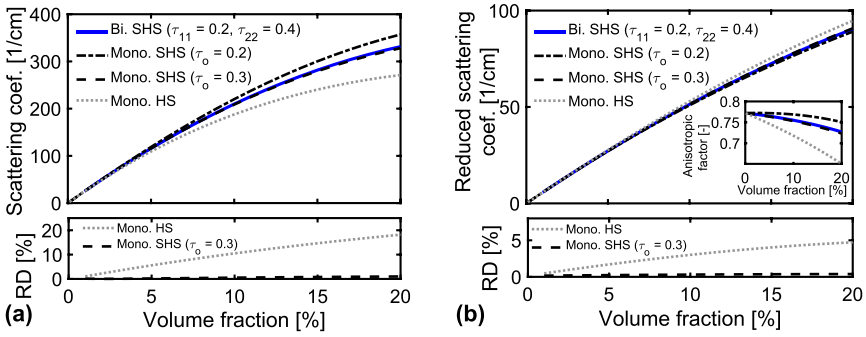

Fig. 6. Scattering properties using the DST with the SHS and HS models in bidisperse stickiness (constant particle size and different stickiness parameters) at $d_1 = d_2 = 500$ nm: (a) Scattering coefficient and (b) Reduced scattering coefficient (anisotropic factor as the inset). The relative differences (RD) based on the bidisperse SHS model are plotted at the bottom. The particle size, particle fraction, and stickiness parameters are the same as in Fig. 4(a).

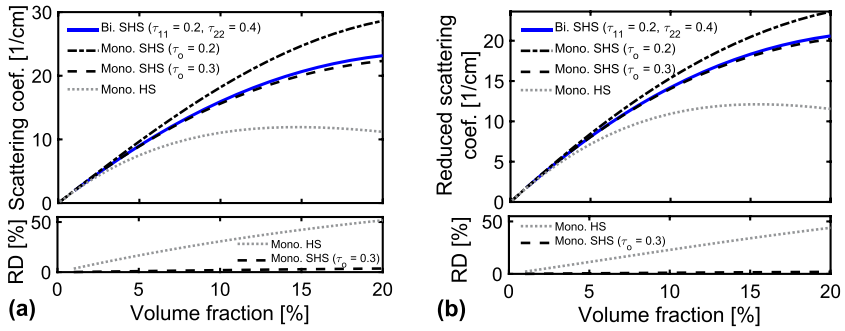

Fig. 7. Scattering properties in bidisperse stickiness at $d_1 = d_2 = 130$ nm. The other details are the same as in Fig. 6.

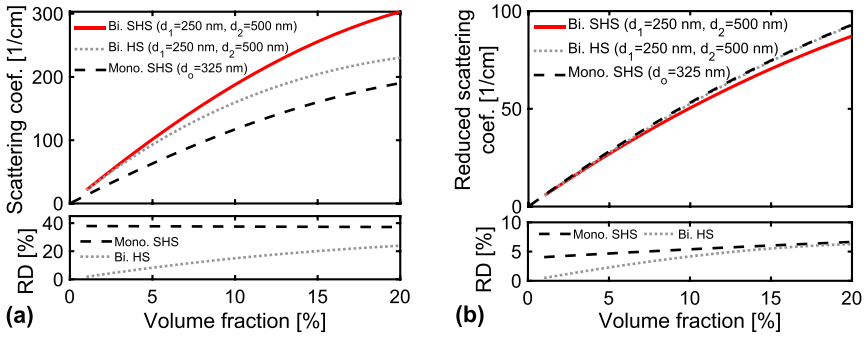

Fig. 8. Scattering properties using the DST with the SHS and HS models in bidisperse particle sizes (different particle sizes and constant stickiness parameter) at $\tau_o = 0.2$. The particle size and fraction, and stickiness parameters are the same as in Fig. 5(b). For monodisperse SHS results, the mean diameter of 325 nm is used.

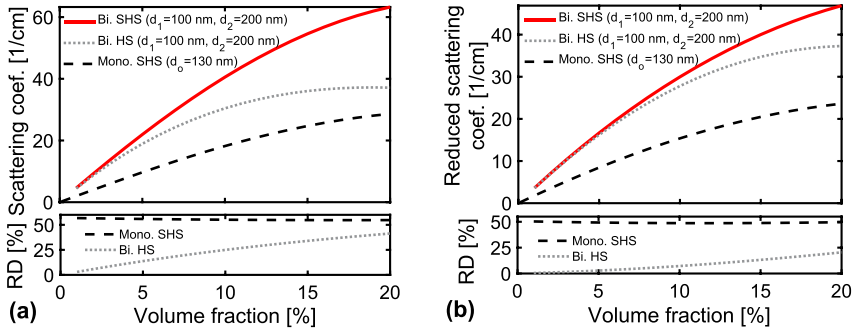

Fig. 9. Scattering properties calculated from the DST with the SHS and HS models in bidisperse particle sizes at the small particle sizes (mean diameter of 130 nm). The other details are the same as Fig. 8.

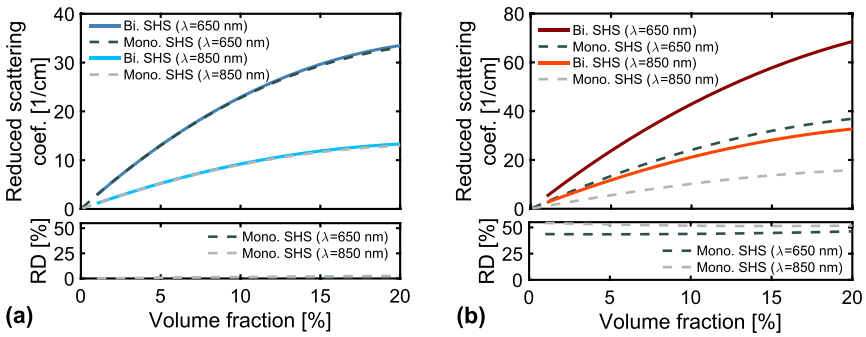

Fig. 10. Reduced scattering coefficients at $\lambda = 650$ and 850 nm wavelengths for the two polydispersities: (a) bidisperse stickiness and (b) bidisperse particle size. Physical parameters, except for the wavelengths, are the same as those in Figs. 7 and 9, respectively. Monodisperse results used mean values of (a) the stickiness parameter and (b) particle sizes.

fraction region. This result is ascribed to the small value of $1 - g$, as in the bidisperse stickiness case.

We examined the effect of bidisperse particle sizes on the scattering properties at small particle sizes ($d_1 = 100$ nm, $d_2 = 200$ nm) in Fig. 9. In the scattering coefficient (Fig. 9(a)), the RDs between models are more significant than those at the large particle sizes (Fig. 8(a)). Even in the reduced scattering coefficient (Fig. 9(b)), the results are different from each model. The RDs between bidisperse HS and SHS models approach approximately 25%.

Wavelength dependence

This section investigated the wavelength dependence of the two polydisperse effects. We focused on the results of the reduced scattering coefficient at the wavelengths of 650 and 850 nm because the scattering coefficient results showed the same trend.

Fig. 10(a) shows the numerical results using the bidisperse and monodisperse SHS models for the polydisperse stickiness case under the same conditions as in Fig. 7 except for the wavelength. At the shorter wavelength (650 nm), the coefficient is larger. The size parameter roughly explains this result; the shorter wavelength corresponds to the larger particle case. The results using the monodisperse SHS model with the mean value of the stickiness parameter agree with those using the bidisperse SHS model at both wavelengths. This agreement indicates that the reduction of the polydisperse stickiness contribution to the monodisperse contribution little depends on the wavelength. Fig. 10(b) shows the numerical results for the polydisperse particle size case under the same condition as those in Fig. 9 except for the wavelength. Unlike the polydisperse stickiness case, the monodisperse SHS model's results largely differ from the bidisperse SHS model. The difference is more significant at the longer wavelength (850 nm), suggesting strong influences of the polydisperse particle size.

Conclusions

We numerically examined polydispersities in stickiness and particle sizes on the light scattering properties (scattering and reduced scattering coefficients) of dense colloidal suspensions up to the volume fraction of 20% using the four particle interaction models: the bidisperse and monodisperse SHS and HS models.

We showed that contributions of polydisperse stickiness are effectively reduced to the monodisperse contribution with the mean value of the polydisperse stickiness parameters on the scattering properties. However, the polydispersity influences the SSF or TCF results. Meanwhile, polydisperse particle sizes strongly influence the scattering properties, and the polydisperse contribution cannot be reduced to the monodisperse contribution. This result is ascribed to the fact that this polydispersity influences the interference in the whole scattering angle region. We also showed that, at the small particle size (130 nm), the scattering properties strongly depend on the particle interaction models, even for the reduced scattering coefficient, which characterizes diffusive radiative transfer. These results suggest that the polydisperse SHS model with different particle sizes and constant stickiness is appropriate for describing the relation between particle configuration change by agglomeration and light scattering. The two polydisperse effects depend less on the optical wavelength in the region from 650 to 850 nm.

Our findings will help attain a systematic understanding of particle agglomeration on the scattering properties in polydisperse colloidal systems and non-destructively evaluate the agglomeration degree even in a dense state by light scattering techniques, such as diffuse optical tomography and photon density wave spectroscopy. In the evaluation, our developed model can be helpful to an inverse analysis.

An experimental investigation of particle agglomeration's effect on the scattering properties is crucial in future work. For example, a comparative study of the scattering properties for the polydisperse SHS model with measurement data is significant for validating the SHS model. To the best of our knowledge, measurement data of the scattering properties in a polydisperse agglomerate system at different volume fractions has not been reported. This paper focused on particle agglomeration in a static state and static particle configuration change via the SSF. Meanwhile, modeling agglomeration in a dynamic state and temporal change of the scattering properties are crucial to evaluating agglomeration's kinetic reaction rate. Such kinetic modeling will be helpful in future work.

CRediT authorship contribution statement

Hiroyuki Fujii: Writing – original draft, Software, Investigation, Funding acquisition, Conceptualization. **Koyata Nishikawa:** Writing – review & editing, Methodology, Investigation. **Hyeonwoo Na:** Writing – review & editing, Software, Investigation, Formal analysis. **Kazumichi Kobayashi:** Writing – review & editing, Supervision. **Masao Watanabe:** Writing – review & editing, Supervision.

Declaration of Generative AI and AI-assisted technologies in the writing process

During the preparation of this work, the authors used "Grammarly" in order to improve language and readability. After using this tool/service, the authors reviewed and edited the content as needed and take full responsibility for the content of the publication.

Declaration of competing interest

The authors declare the following financial interests/personal relationships which may be considered as potential competing interests: Hiroyuki Fujii reports a relationship with Japan Association for Chemical Innovation that includes: funding grants. Hiroyuki Fujii reports a

relationship with Japan Society for the Promotion of Science London that includes: funding grants. Hiroyuki Fujii reports a relationship with Nakatani Foundation for Advancement of Measuring Technologies in Biomedical Engineering that includes: funding grants. If there are other authors, they declare that they have no known competing financial interests or personal relationships that could have appeared to influence the work reported in this paper.

Acknowledgments

The first author (H.F.) would like to thank members of Prof. L. Tsang's group for supporting his visit to the University of Michigan. The authors would like to thank Mr. H. Nozaki, R. Sawada, and S. Sasaki for the fruitful discussion. H.F. acknowledges financial support from the 11th JACI Prize for Encouraging Young Researcher, Grant-in-Aid for Scientific Research, Japan (22KK0243) of the Japan Society for the Promotion of Science, KAKENHI, and the Nakatani Foundation, Japan.

Data availability

Data will be made available on request.

References

[1] Pogue BW, Patterson MS. Review of tissue simulating phantoms for optical spectroscopy, imaging and dosimetry. J Biomed Opt 2006;11(4):041102. http://dx.doi.org/10.1117/1.2335429, 1–16.
[2] Masumi S, Senba E. Nitric oxide involvement in lipid emulsion-induced vascular pain in anesthetized rats. Eur J Pharmacol 2008;594:64–9. http://dx.doi.org/10.1016/j.ejphar.2008.07.01.
[3] Onishi M, Koyama Y, Hagika A, Omotani S, Hatsuda Y, Maezaki N, Myotoku M. Effect of central venous nutrition infusion, , intravenous fat emulsion, and therapeutic agents on the particle size of fat emulsion for simultaneous administration of three drugs. Ann Nutr Metab 2022;78(6):307–15. http://dx.doi.org/10.1159/000526329.
[4] Ma L, Li B, Han F, Yan S, Wang L, Sun J. Evaluation of the chemical quality traits of soybean seeds, as related to sensory attributes of soymilk. Food Chem 2015;173:694–701. http://dx.doi.org/10.1016/j.foodchem.2014.10.09.
[5] Saito Y, Konagaya K, Suzuki T, Kondo N. Determination of optical coefficients of tofu using spatially resolved diffuse reflectance at 633 nm. Eng Agric Env Food 2018;11(1):38–42. http://dx.doi.org/10.1016/j.eaef.2017.12.001.
[6] Zhao Z, Corredig M. Colloidal properties of casein micelles suspensions as a function of pH during concentration by osmotic stressing. Food Hydrocoll 2016;60:445–52. http://dx.doi.org/10.1016/j.foodhyd.2016.04.016.
[7] Tiarks F, Frechen T, Kirsch S, Leuninger J, Melan M, Pfau A, Richter F, Schuler B, Zhao CL. Formulation effects on the distribution of pigment particles in paints. Prog Org Coat 2003;48:140–52. http://dx.doi.org/10.1016/S0300-9440(03)00095-X.
[8] Yan Z, Zhao L, Kong X, Hua Y, Chen Y. Behaviors of particle size and bound proteins of oil bodies in soymilk processing. Food Chem 2016;194:881–90. http://dx.doi.org/10.1016/j.foodchem.2015.08.100.
[9] Mahmoud B, Rice HP, Mortimer L, Fairweather M, Harbottle D. Acoustic method for determination of the thermal properties of nanofluids. Ind Eng Chem Res 2019;58:19719–31. http://dx.doi.org/10.1021/acs.iecr.9b02983.
[10] Buzzaccaro S, Rusconi R, Piazza R. Sticky hard spheres: Equation of state, phase diagram, and metastable gels. Phys Rev Lett 2007;99:098301. http://dx.doi.org/10.1103/PhysRevLett.99.098301.
[11] Duits MH, May RP, Vrij A, de Kruif CG. Small-angle neutron scattering of concentrated adhesive-hard-sphere dispersions. Langmuir 1991;7(1):62–8. http://dx.doi.org/10.1021/la00049a014.
[12] Woutersen AT, May RP, de Kruif CG. The equilibrium microstructure of adhesive hard sphere dispersions: A small-angle neutron scattering study. J Colloid Interface Sci 1992;151(2):410–20. http://dx.doi.org/10.1016/0021-9797(92)90490-D.
[13] Pellegrino F, Pellutiè L, Sordello F, Minero C, Ortel E, Hodoroaba VD, Maurino V. Influence of agglomeration and aggregation on the photocatalytic activity of TiO2 nanoparticles. Appl Catal B: Env 2017;216:80–7. http://dx.doi.org/10.1016/j.apcatb.2017.05.046.
[14] Gripon C, Legrand L, Rosenman I, Boué F, Regnaut C. Relation between the solubility and the effective solute-solute interaction for C60 solutions and lysozyme solutions: A comparison using the sticky hard-sphere potential. J Cryst Growth 1998;183:258–68. http://dx.doi.org/10.1016/S0022-0248(97)00416-8.
[15] Chen Y, Ono T. Protein particle and soluble protein structure in prepared soymilk. Food Hydrocoll 2014;39:120–6. http://dx.doi.org/10.1016/j.foodhyd.2014.01.005.
[16] Cousin F, Dubois E, Cabuil V. Approach of the critical point of gas-liquid transitions in an electrostatically stabilized colloidal suspension. J Chem Phys 2001;115(13):6051–7. http://dx.doi.org/10.1063/1.1400128.
[17] Yang B, Huang P, Song S, Luo H, Zhang Y. Hydrophobic agglomeration of apatite fines induced by sodium oleate in aqueous solutions. Results Phys 2018;9:970–7. http://dx.doi.org/10.1016/j.rinp.2018.03.049.
[18] Ghasemifard M, Abrishami ME, Iziy M. Effect of different dopants Ba and Ag on the properties of SrTiO3 nanopowders. Results Phys 2015;5:309–13. http://dx.doi.org/10.1016/j.rinp.2015.10.005.
[19] Li C, Jiang H. Imaging of particle size and concentration in heterogeneous scattering media using multispectral diffuse optical tomography. Opt Express 2004;12(25):6313–8. http://dx.doi.org/10.1364/OPEX.12.006313.
[20] Bressel L, Hass R, Reich O. Particle sizing in highly turbid dispersions by photon density wave spectroscopy. J Quant Spectrosc Radiat Transfer 2013;126:122–9. http://dx.doi.org/10.1016/j.jqsrt.2012.11.031.
[21] Cartigny JD, Yamada Y, Tien CL. Radiative transfer with dependent scattering by particles: part 1 - theoretical investigation. J Heat Transf 1986;108:608–13. http://dx.doi.org/10.1115/1.3246979.
[22] Yamada Y, Cartigny JD, Tien CL. Radiative transfer with dependent scattering by particles: Part 2 - experimental investigation. J Heat Transf 1986;108:614–8. http://dx.doi.org/10.1115/1.3246980.
[23] Nguyen VD, Faber DJ, van der Pol E, van Leeuwen TG, Kalkman J. Dependent and multiple scattering in transmission and backscattering optical coherence tomography. Opt Express 2013;21(24):29145–56. http://dx.doi.org/10.1364/OE.21.029145.
[24] Fujii H, Tsang L, Zhu J, Nomura K, Kobayashi K, Watanabe M. Photon transport model for dense polydisperse colloidal suspensions using the radiative transfer equation combined with the dependent scattering theory. Opt Express 2020;28(15):22962–77. http://dx.doi.org/10.1364/OE.398582.
[25] Ma LX, Wang CC, Tan JY. Light scattering by densely packed optically soft particle systems, with consideration of the particle agglomeration and dependent scattering. Appl Opt 2019;58(27):7336–45. http://dx.doi.org/10.1364/AO.58.007336.
[26] Chang W, Ding KH, Tsang L, Xu X. Microwave scattering and medium characterization for terrestrial snow with QCA-Mie and bicontinuous models: Comparison studies. IEEE Trans Geosci Remote Sens 2016;54(6):3637–48. http://dx.doi.org/10.1109/TGRS.2016.2522438.
[27] Tsang L, Kong JA, Ding K-H, Ao CO. Scattering of electromagnetic waves: numerical simulations. John Wiley & Sons, Ltd; 2001.
[28] Grody N. Relationship between snow parameters and microwave satellite measurements: Theory compared with advanced microwave sounding unit observations from 23 to 150 GHz. J Geophys Res 2008;113(22):D22108. http://dx.doi.org/10.1029/2007JD009685, 1–17.
[29] Ntziachristos V. Going deeper than microscopy: The optical imaging frontier in biology. Nat Methods 2010;7(8):603–14. http://dx.doi.org/10.1038/nmeth.1483.
[30] Tuchin VV. Tissue optics : Light scattering methods and instruments for medical diagnosis. SPIE Press; 2015.
[31] Wang LV, Wu H. Biomedical optics: Principles and imaging. John Wiley & Sons, Ltd; 2009.
[32] Bohren CF, Huffman DR. Absorption and scattering of light by small particles. John Wiley & Sons; 1983.
[33] Hunter RJ. Foundations of colloid science. New York: Oxford University Press Inc.; 2001.
[34] Hansen J-P, McDonald I. Theory of simple liquids. Elsevier; 2006.
[35] Fujii H, Ueno M, Inoue Y, Aoki T, Kobayashi K, Watanabe M. Model equations of light scattering properties and a characteristic time of light propagation for polydisperse colloidal suspensions at different volume fractions. Opt Express 2022;30(3):3538–52. http://dx.doi.org/10.1364/OE.447334.
[36] Fujii H, Na H, Yi J, Kobayashi K, Watanabe M. Particle size distribution effects on the light scattering properties in non-diluted colloidal suspensions: A numerical study. Colloids Surf A: Physicochem Eng 2024;703(135208):1–9. http://dx.doi.org/10.1016/j.colsurfa.2024.135208.
[37] Percus JK, Yevick GJ. Analysis of classical statistical mechanics by means of collective coordinates. Phys Rev 1958;110(1):1–13. http://dx.doi.org/10.1103/PhysRev.110.1.
[38] Baxter RJ. Ornstein–Zernike relation and Percus–Yevick approximation for fluid mixtures. J Chem Phys 1970;52(9):4559–62. http://dx.doi.org/10.1063/1.1673684.
[39] Gehin C, Persello J, Charraut D, Cabane B. Electrorheological properties and microstructure of silica suspensions. J Colloid Interface Sci 2004;273(2):658–67. http://dx.doi.org/10.1016/j.jcis.2004.01.029.
[40] van Staveren HJ, Moes CJM, van Marie J, Prahl SA, van Gemert MJC. Light scattering in intralipid-10 % in the wavelength range of 400-1100 nm. Appl Opt 1991;30(31):4507–14. http://dx.doi.org/10.1364/AO.30.004507.